Fully Guided Synthetic Osteochondral Resurfacing of a Large Stifle OCD Lesion Using a Patient-Specific Implant and Drill Guides

Jasmine Moser[1]   Georg Haimel[2]   Karen Barker-Benfield[3]   Katharina Leschnik[4]   Peter Böttcher[5]

[1] Fitzpatrick Referrals Oncology and Soft Tissue, Guildford, United Kingdom
[2] Tierarztpraxis am Stadtpark, Vienna, Austria
[3] Tierphysio Rodaun, Vienna, Austria
[4] AniCura Tierklinik Hollabrunn, Hollabrunn, Austria
[5] Small Animal Clinic, Division for Surgery, FU-Berlin, Berlin, Germany

Address for correspondence Peter Böttcher, DVM, Klein- und Heimtierklinik, Oertzenweg 19 b, D 14163 Berlin, Germany (e-mail: peter.boettcher@fu-berlin.de).

Abstract

Synthetic anatomical reconstruction of extensive, oval osteochondrosis dissecans (OCD) defects remains a challenge due to the 'one shape fits all' design of commercial round implants. This is further complicated by the inherent inaccuracy of free-hand implant positioning procedures. A 6-month-old German Shepherd presented with a $15 \times 7.8 \times 4.3$ mm OCD defect at the lateral femoral condyle. A synthetic patient-specific implant (PSI) was designed, using the contralateral unaffected condyle as a template. Reaming of the implant bed was fully guided using a set of three-dimensional-printed drill guides. The implant, consisting of a titanium base and a polycarbonate urethane bearing surface, was press-fit into place. Temporary meniscal release of the cranial meniscal horn was repaired, followed by routine closure and postoperative care. The combination of PSI and matching drill guides resulted in an accurate restoration of the normal joint surface at the former defect area. At 6-week and 18-month follow-ups, mild joint effusion, unexpected soft tissue mineralization and a small joint mouse were present. No other complications were encountered, and the dog was clinically lameness-free. At 6 weeks and 6 months, computerized gait analysis documented increased loading of the affected limb from 36% preoperatively to 42 and 40%, on follow-up, respectively. Body weight distribution between both hindlimbs was nearly equal at the 6-month control with 1% difference in loading. Osteochondral resurfacing using a PSI appears to be a promising treatment option for large stifle OCD lesions in which other treatment modalities may not be eligible.

Keywords
► OCD
► stifle
► resurfacing
► patient-specific

Introduction

Surgical management of osteochondrosis dissecans (OCD) lesions is multifaceted, aiming for pain relief, restoration of joint surface integrity, as well as prevention of secondary osteoarthritis. Previously employed surgical techniques in canine stifle OCD include debridement and induction of fibrocartilage scar formation,[1,2] osteochondral allo- and autograft transplantation,[3–7] and synthetic osteochondral resurfacing (SOR).[8,9] Debridement up to the point of subchondral bleeding is considered standard care for OCD lesions in canines.[1,2,10] However, the resultant fibrous

cartilage lacks the strength of hyaline cartilage necessary to restore normal pressure distribution,[11] preventing the development of secondary 'kissing lesions' on the opposing joint surface,[12] or rim stress concentration around the primary defect.[13] This lack of structural strength and persistent joint incongruity leads to mixed functional results and the progression of osteoarthritis, especially with large defects.[1,2] Advanced resurfacing techniques, such as osteochondral autograft transplantation (OAT) and SOR, could potentially overcome the aforesaid shortcomings of standard OCD treatment,[4,5,7–9,14] but some limitations must be considered. Osteochondral autograft transplantation is restricted by donor site availability, donor site morbidity and unimpeded biological integration of the transplant.[4,5,7,14] Synthetic osteochondral resurfacing is limited by the size and shape of commercially available implants, which do not exactly match the narrow axial–abaxial dimension and curvature of the lateral femoral condyle. In case of a biphasic design with a metallic base and a polymer gliding surface, an overlapped implant configuration is not possible, limiting the use of SOR to predominantly round defects. A patient-specific SOR implant would overcome those limitations. The aim of this case report is to describe the surgical procedure, complications and functional outcome in a dog treated with a patient-specific SOR, in combination with intraoperative navigation, for an extended focal OCD defect at the lateral femoral condyle.

Case Description

Preoperative Assessment

A 6-month-old, 27 kg, intact female German Shepherd presented with a grade II/V left hindlimb (LHL) lameness. Pain was elicited upon extension and flexion of the left stifle with marked joint effusion on palpation. Orthogonal radiographs of both stifles showed a marked subchondral bone defect with flattening of the lateral femoral condyle on the left stifle, consistent with an OCD lesion (►**Fig. 1A**). Subsequent axial computed tomography (Somatom Emotion 6, Siemens Healthcare GmbH, Erlangen, Germany) confirmed the diagnosis of a large OCD lesion measuring $15.0 \times 7.8 \times 4.3$ mm $(L \times W \times H)$ (►**Fig. 2**).

Fig. 1 Pre- and postoperative stifle radiographs. (A) Note the subchondral defect and surrounding sclerosis at the lateral femoral condyle in the preoperative image; (B) immediate postoperative image, documenting proper seating of the patient-specific implant (PSI); (C) 6 weeks postoperative, with evidence of moderate joint effusion and a small bony fragment in the caudal joint pouch. PSI position unchanged, but a small halo appears around the base plate, indicating delayed bony incorporation. The halo around the polycarbonate urethane (PCU) cup is a normal finding, because PCU never bonds to bone; (D) 18-month follow-up: PSI position unchanged and bone-to-metal contact at the bottom of the socket. Persistent joint effusion and significant proliferation of the fragment in the caudal joint pouch. In addition, bone metaplasia is visible laterally and craniolaterally (confirmed by computed tomography).
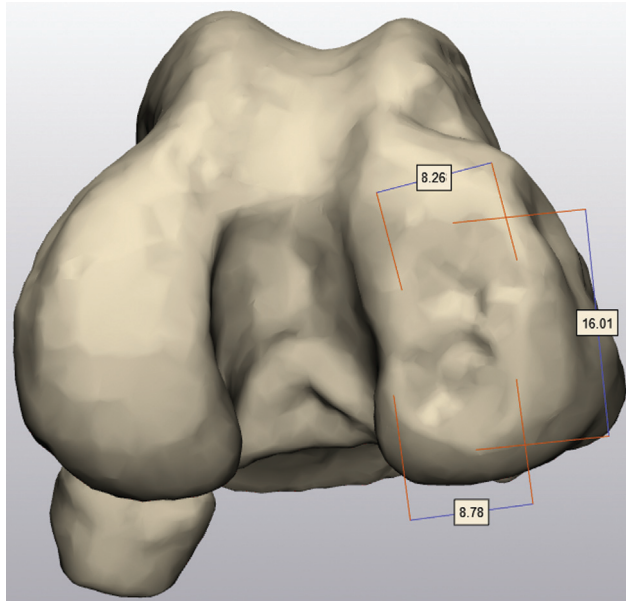
Fig. 2 Computed tomography three-dimensional rendering of distal left femur. Note the extent of the osteochondrosis dissecans lesions covering almost the entire condylar surface, measuring over 15 mm in length and 8 mm in width.

Patient-Specific Implant and Surgical Templates

The custom-made implant comprised a titanium base and a polycarbonate urethane (PCU) bearing cup, similar to commercially available implants.[9] Three-dimensional (3D) modelling of the implant was based on the axial CT images of both stifles using dedicated software (Mimics Innovation Suite, Materialise, Leuven, Belgium) and the unaffected right lateral femur as a template (►Fig. 3). To promote bone ingrowth as well as firm bonding between the PCU and the base, lattices were added to the metallic base, which was cast in medical-grade titanium (DOR-A-MATIC, Schütz Dental GmbH, Rosbach, Germany). The bearing cup was overmoulded onto the titanium base with PCU (Carbothane AC-4085A, The Lubrizol Corporation, Wilmington, Massachusetts, United States).

Additionally, two sets of drill and reaming templates/guides and trial implants were 3D-printed, allowing for full guidance during the in vivo procedure. Additionally, 3D models of the affected distal femur with the OCD defect and sham implants were provided to allow for dry-lab practice.

Surgery

The dog was positioned in dorsal recumbency and stabilized with a vacuum bag to allow unrestricted movement/flexion of the affected limb. An extended lateral parapatellar approach was used. Access to the most caudal extent of the defect necessitated temporary release of the cranial horn of the lateral meniscus, by transection of the intermeniscal and cranial meniscotibial ligament. Subsequently, using the provided 3D-printed three-hole drill guide (►Fig. 4A), three 2.4 mm guide pins were placed until the caudal cortex of the condyle was reached. With the proximal pin reintroduced, serving as a guide for a 6 mm cannulated counterbore reamer (Cannulated Headed Reamer, Arthrex VetSystem, Munich, Germany), reaming was executed to the precalculated depth, controlled using the laser marks on the reamer. The reaming process was repeated for the central and distal holes, using an 8 mm counterbore reamer. Correct reaming depth was verified using a trial implant (►Fig. 4B, C). The only PSI was inserted with a tamp to its final position (►Fig. 4D). The meniscal release was repaired with 3-0 polydioxanone using a locking-loop suture both for the intermeniscal and meniscotibial ligaments. Routine closure of the surgical site was performed. Recorded surgery time was 135 minutes.

Postoperative Management and Clinical Follow-Up

The dog was discharged the day after surgery, with carprofen and gabapentin, for 2 and 4 weeks, respectively, showing a grade IV/V lameness. Cage rest and short leash-only walks were advised for a period of 6 weeks.

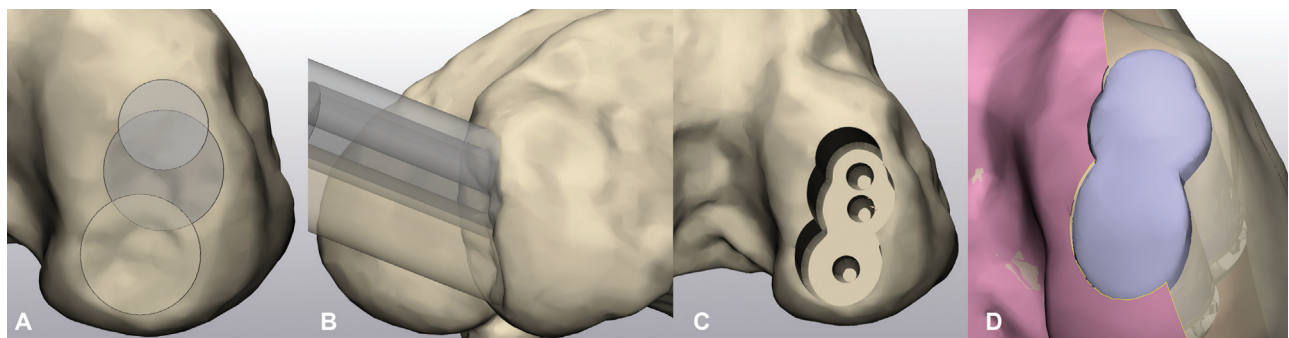Wound healing was uneventful, and no clinical complications were reported.

Fig. 3 In-silico planning of patient-specific implant (PSI) and extraction of PSI geometry. (A) Lesion fully covered using overlapping cylinders of various diameters; (B) trajectory of virtual reamers (cylinders) checked to ensure unrestricted access during in vivo reaming (avoiding potential conflict with tibial plateau) and position not perfectly orthogonal to the joint surface, compared to osteochondral transplantation; (C) situation following virtual reaming of implant bed; (D) PSI geometry extracted from matching contralateral condyle (*pink*) using virtual reamers. Note that the rim of the PSI gliding surface is not flush with the surrounding joint surface at the narrowing, as this would disrupt the geometrical continuity of the condylar PSI curvatures.
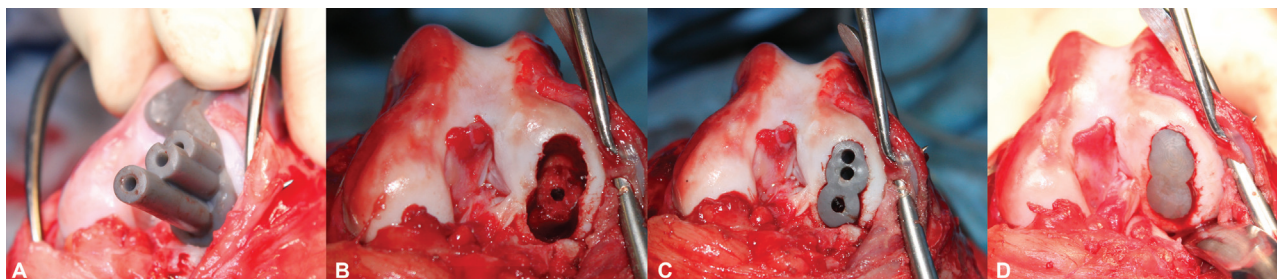
Fig. 4 Intraoperative images of the key steps of navigated patient-specific implant (PSI). (A) Surgical template applied for placement of three 2.4 mm guide pins; (B) prepared implant bed, using guide pins for precise guidance of cannulated 6 and 8 mm reamers; (C) template used to verify correct reaming depth; (D) PSI press-fit into position. Note the restoration of physiological joint contours as well as flush seating of the polycarbonate urethane gliding surface with respect to the surrounding joint cartilage.

After 6 weeks, the dog exhibited a grade II/V lameness, and was comfortable upon manipulation of the stifle. At 6 months, no lameness was visible.

At 18 months, a slightly reduced range of motion, moderate periarticular fibrosis and mild discomfort during hyperflexion were elicited. Arthrocentesis for cytology and bacterial culture was performed. The cytological examination was consistent with mild osteoarthritis. The bacterial culture was negative.

Follow-Up Imaging

Immediate postoperative radiographs revealed appropriate implant placement (►**Fig. 1B**). At 6 weeks, the implant position remained unchanged, with mild peri-implant sclerosis and thin halo around the titanium base, suspicious for unsuccessful bony on- and ingrowth (►**Fig. 1C**). Alternatively, an Überschwinger artefact cannot be ruled out completely. Additionally, a 3×1.5 mm bony fragment in the caudal joint pouch was visible on the lateral view. No osteoarthritic changes were noted but mild joint effusion was present. After 18 months, radiographs showed mild osteophyte formation, suggestive of beginning gonarthrosis. The implant base appeared to be fully integrated, without the previously seen halo. Peri-implant sclerosis remained unchanged, as well as joint effusion. The bony fragment in the caudal joint pouch had proliferated. Additionally, heterotopic bone formations in the cranial compartment were present. These findings were further evaluated by computed tomography. Stable implant position and bony integration were confirmed. The bony proliferations in the cranial and craniolateral compartment were most likely located within the joint capsule, measuring $7 \times 2.5 \times 4$ mm (cranial) and $16 \times 3 \times 4$ mm (lateral). The bony fragment within the caudal joint pouch, measuring $10 \times 3 \times 10$ mm, could not be attributed to any definite origin.

Gait Analysis

Five days before surgery, 6 weeks and 6 months postoperatively, computerized gait analysis was performed with a pressure-sensitive treadmill specifically designed for dogs (CanidGait; zebris Medical GmbH, Isny, Germany). The system consists of a treadmill equipped with a calibrated pressure sensor matrix and two synchronized cameras.

The matrix dimensions are 163×41 cm, equipped with 9,216 high precision, individually calibrated, capacitive pressure sensors with a scanning rate of 100 Hz. During data acquisition, speed was set to 4 km/h. Parameters evaluated in all four limbs included peak pressure/force distribution, expressed as a percentage of body weight and body load distribution (centre of pressure).

Preoperatively, the affected LHL was loaded the least (36% body weight versus 39% on the right hindlimb (RHL) and 66 versus 64% for the left (LFL) and right forelimb (RFL) respectively. Going from pre- to 6 weeks postoperatively the pressure distribution decreased in the forelimbs and increased in the rear limbs (LHL 42% vs. RHL 45%; LFL 65% vs. RFL 63%), with the left hindlimb not fully loaded. At 6 months there was a further symmetrical decrease in forelimb loading (LFL 64 vs. RFL 62%), while hindlimb loading was now greater in the affected left limb (LHL 40 vs. RHL 39%). Preoperatively and 6 weeks postoperatively, the centre of pressure was shifted to the RHL. At 6 months, the centre of pressure was centred, indicating a balanced, symmetrical gait. No computerized gait analysis was performed at the 18 months follow-up, as the owner did not consent.

Discussion

This is the first report describing fully guided resurfacing of a large stifle OCD lesion with a synthetic PSI in dogs. Lameness became clinically undetectable at 6 months, which was also verified by computerized gait analysis. Feedback from the owner was positive as the dog regained a normal level of physical activity, without any signs of lameness or discomfort, even after strenuous exercise. No minor or major complications were encountered. Whether the bony proliferations documented at the 18-month follow-up are of clinical significance shall be monitored closely.

As large condylar lesions are oval, the shelf round implants hardly ever match the lesion, which results in fibrocartilaginous repair in the surface areas uncovered by the implant.[9] Mediolateral oversizing aiming for as much coverage along the longitudinal axis as possible would not have been an option in the current case as the mediolateral dimension of the condyle only measured 14 mm; hence, the application of a Ø15 mm resurfacing implant would not have been feasible. Placing two smaller implants immediately

adjacent to each other would not be a safe solution either, because the SOR implants need a discrete osseous bridge for bone integration all around. As mentioned earlier, overlapping two or more SOR implants, which is a standard surgical technique with OAT,[4,7,14] is not possible either because of the titanium base. Lastly, both OAT and available SOR cannot accurately fit the curvature of the condyle, stimulating joint degeneration as well as accelerated implant wear.

The advantages of using a PSI in combination with patient-specific guides were deemed to be manifold: firstly, an accurate replica of the joint surface could be developed; secondly, preoperative planning and the production of patient-specific drill guides would allow for a fully navigated procedure and therefore reduce the risk of mal-angulation and related joint incongruence; thirdly, virtual planning could be rehearsed on a 1:1 model and replicated 1:1 in surgery. The decision to use a PCU surface layer was based on previous studies showing that PCU is resistant to surface degradation and fissuring and has excellent wear and bearing properties when used in a unipolar configuration,[9,15–17] as well as causing minimal damage to the opposing articulating normal hyaline cartilage in a typical OCD setting.[8,9,17] This is of particular importance, since contact mechanics of PCU against a rough surface, such as an arthritic joint surface, both exhibit and induce accelerated wear.[18]

Navigated resurfacing has already been described with positive outcomes in humans and laboratory animals.[19–22] Comparisons between several studies showed that surgical guides improved the surgical outcome and decreased surgery time.[23] As in our case, the use of surgical guides resulted in a straightforward procedure and exact implant placement. In addition, we believe that the dry-lab session prior to the procedure using bone models, drill guides and implants contributed significantly to the positive outcome.

The large volume of osseous metaplasia found at the last follow-up in the craniolateral and lateral compartments might be a consequence of meniscal trauma, resulting from temporary release. Probably more important is the potential impairment of meniscal function associated with temporary release. Loss of lateral meniscal function may alter lateral compartmental contact mechanics to a much greater degree than an untreated OCD defect,[24] potentially reversing the benefits of PSI resurfacing. Although the ligamentous attachments were reanastomosed and meniscal fixation appeared stable on palpation, there is a risk of suture strength loss and overall impairment of lateral meniscal function. Future applications should investigate transosseous suture fixation, bone anchors or bone plug fixation, which seems to be the most efficient fixation method.[25,26]

At the 18-month radiographic follow-up, stable fixation of the PSI with evidence of bony incorporation was present. Previous studies in a sheep model using similar implants showed bone-to-implant contact already at 6 months.[27] However, delayed osseous integration of up to 2 years due to some degree of persistent (micro)instability was documented in a human study after customized resurfacing.[28]

In our case, the large surface area of the PSI probably exposes the implant to increased shear forces during articu-lation. Subsequently, the risk of mechanical loosening and delayed integration increases. To counteract those risks, the implant was designed to be seated more deeply in the host bone (13 mm) compared to the SynACART implants (8 mm).[9] Additionally, a peg, enhancing resistance against pivoting moments, was added.

To further eliminate the risks of delayed osseointegration and (micro-)instability, the following should be considered in the future: optimization of the 'open-pore' design for the base of the implant as well as core reamers with a flat tip allowing for close contact between the base and the host bone immediately following implantation.

As with most single case reports, conclusions should be drawn with caution. Especially regarding the long-term performance of the PSI, the follow-up period of 18 months is certainly too short to observe every complication typically associated with synthetic implants, such as wear, overall mechanical failure of the implant or septic/aseptic loosening. When dealing with unipolar resurfacing, as in the present case, implant-related cartilage degeneration at the opposing joint surface ought to be added to the list. The observed persistent joint effusion could be a sign of detritic synovitis related to PCU wear debris or implant-induced meniscal and/or cartilage damage at the tibial plateau.[8,29] Because absence of visible PCU debris on cytology does not rule out such debris formation, further studies are needed to clarify this point. Nevertheless, synovitis could also be attributed to some mechanical irritation arising from the osseous proliferations.

Despite these limitations, this report describes a novel method for the successful correction of a large OCD lesion using a double-layer PSI. Although progression of osteoarthritis has been observed, in cases where OAT and standard SOR are not deemed feasible, patient-specific synthetic resurfacing allows for precise repair of complex OCD defects, thus dispensing with concerns over donor site availability and morbidity. The procedure itself is technically straightforward, allows early return to function and costs can be maintained at a comparable level of standard SOR implants.

Authors' Contributions

Haimel was the surgeon in lead, Böttcher planned and provided the implant and associated drill guides, Leschnik was involved in clinical case management, Barker-Benfield performed the gait analyses, and Moser wrote the main draft of the publication, which was reviewed and edited by all authors until final approval.

Conflict of interest

None declared. Böttcher may receive royalties, once the reported implant system may become a commercial product.

References

1 Harari J. Osteochondrosis of the femur. Vet Clin North Am Small Anim Pract 1998;28(01):87–94
2 Bertrand SG, Lewis DD, Madison JB, de Haan JH, Stubbs WP, Stallings JT. Arthroscopic examination and treatment of

osteochondritis dissecans of the femoral condyle of six dogs. J Am Anim Hosp Assoc 1997;33(05):451–455

3 Fitzpatrick N, Yeadon R, Smith TJ. Early clinical experience with osteochondral autograft transfer for treatment of osteochondritis dissecans of the medial humeral condyle in dogs. Vet Surg 2009; 38(02):246–260

4 Fitzpatrick N, Yeadon R, van Terheijden C, Smith TJ. Osteochondral autograft transfer for the treatment of osteochondritis dissecans of the medial femoral condyle in dogs. Vet Comp Orthop Traumatol 2012;25(02):135–143

5 Frank M. Use of osteochondral grafting for therapy of osteochondrosis dissecans (ocd) in the canine knee joint. description of the technique and preliminary results following the treatment of five cases]. Tierärztl Prax 2003;31(K):346–355

6 Franklin SP, Stoker AM, Murphy SM, et al. Outcomes associated with osteochondral allograft transplantation in dogs. Front Vet Sci 2021;8:759610. Doi: 10.3389/fvets.2021.759610

7 Cinti F, Vezzoni L, Vezzoni A. A new generation of osteochondral autograft transfer system for the treatment of osteochondritis dissecans of the femoral condyle: clinical experience in 18 dogs. Vet Comp Orthop Traumatol 2022;35(03):198–204 Epub20220311. Doi: 10.1055/s-0042-1744181

8 Cook JL, Kuroki K, Bozynski CC, Stoker AM, Pfeiffer FM, Cook CR. Evaluation of synthetic osteochondral implants. J Knee Surg 2014; 27(04):295–302

9 Egan P, Murphy S, Jovanovik J, Tucker R, Fitzpatrick N. Treatment of osteochondrosis dissecans of the canine stifle using synthetic osteochondral resurfacing. Vet Comp Orthop Traumatol 2018;31 (02):144–152

10 Poulos PW Jr. Canine osteochondrosis. Vet Clin North Am Small Anim Pract 1982;12(02):313–328

11 Nelson B, Anderson D, Brand RA, Brown TD. Effects of osteochondral defect size on cartilage contact stress. Acta Orthop Scand 1988;59(05):574–579

12 Yan W, Xu X, Xu Q, et al. Chondral defects cause kissing lesions in a porcine model. Cartilage 2021;13(2_suppl):692S–702S

13 Guettler JH, Demetropoulos CK, Yang KH, Jurist KA. Osteochondral defects in the human knee: influence of defect size on cartilage rim stress and load redistribution to surrounding cartilage. Am J Sports Med 2004;32(06):1451–1458

14 Cook JL, Hudson CC, Kuroki K. Autogenous osteochondral grafting for treatment of stifle osteochondrosis in dogs. Vet Surg 2008;37 (04):311–321

15 Kanca Y, Milner P, Dini D, Amis AA. Tribological evaluation of biomedical polycarbonate urethanes against articular cartilage. J Mech Behav Biomed Mater 2018;82:394–402

16 Khan I, Smith N, Jones E, Finch DS, Cameron RE. Analysis and evaluation of a biomedical polycarbonate urethane tested in an in vitro study and an ovine arthroplasty model. Part II: in vivo investigation. Biomaterials 2005;26(06):633–643

17 Luo Y, McCann L, Ingham E, Jin ZM, Ge S, Fisher J. Polyurethane as a potential knee hemiarthroplasty biomaterial: an in-vitro simulation of its tribological performance. Proc Inst Mech Eng H 2010; 224(03):415–425

18 Damen AHA, Nickien M, Ito K, van Donkelaar CC. The performance of resurfacing implants for focal cartilage defects depends on the degenerative condition of the opposing cartilage. Clin Biomech (Bristol, Avon) 2020;79:105052

19 Kunz M, Devlin SM, Hurtig MB, et al. Image-guided techniques improve the short-term outcome of autologous osteochondral cartilage repair surgeries: an animal trial. Cartilage 2013;4(02): 153–164

20 Kunz M, Rudan JF. Patient-specific surgical guidance system for intelligent orthopaedics. Adv Exp Med Biol 2018;1093:225–243

21 Sebastyan S, Kunz M, Stewart AJ, Bardana DD. Image-guided techniques improve accuracy of mosaic arthroplasty. Int J CARS 2016;11(02):261–269

22 Koulalis D, Di Benedetto P, Citak M, O'Loughlin P, Pearle AD, Kendoff DO. Comparative study of navigated versus freehand osteochondral graft transplantation of the knee. Am J Sports Med 2009;37(04):803–807

23 Tack P, Victor J, Gemmel P, Annemans L. 3D-printing techniques in a medical setting: a systematic literature review. Biomed Eng Online 2016;15(01):115. Doi: 10.1186/s12938-016-0236-4

24 Choate CJ, Kim SE, Hudson CC, Spreng D, Pozzi A. Effect of lateral meniscectomy and osteochondral grafting of a lateral femoral condylar defect on contact mechanics: a cadaveric study in dogs. BMC Vet Res 2013;9:53

25 Ow ZGW, Cheong CK, Hai HH, et al. Securing transplanted meniscal allografts using bone plugs results in lower risks of graft failure and reoperations: a meta-analysis. Am J Sports Med 2021; 3635465211042014:3635465211042014 Epub20211012. Doi: 10.1177/03635465211042014

26 Kim SH, Lipinski L, Pujol N. Meniscal allograft transplantation with soft-tissue fixation including the anterior intermeniscal ligament. Arthrosc Tech 2019;9(01):e137–e142

27 Martinez-Carranza N, Ryd L, Hultenby K, et al. Treatment of full thickness focal cartilage lesions with a metallic resurfacing implant in a sheep animal model, 1 year evaluation. Osteoarthritis Cartilage 2016;24(03):484–493

28 Stålman A, Sköldenberg O, Martinez-Carranza N, Roberts D, Högström M, Ryd L. No implant migration and good subjective outcome of a novel customized femoral resurfacing metal implant for focal chondral lesions. Knee Surg Sports Traumatol Arthrosc 2018;26(07):2196–2204

29 Smith RA, Maghsoodpour A, Hallab NJ. In vivo response to cross-linked polyethylene and polycarbonate-urethane particles. J Biomed Mater Res A 2010;93(01):227–234